Field-Measurement-Based Received Power Analysis for Directional Beamforming Millimeter-Wave Systems: Effects of Beamwidth and Beam Misalignment

Juyul Lee, Myung-Don Kim, Jae-Joon Park, and Young Jun Chong

To overcome considerable path loss in millimeter-wave propagation, high-gain directional beamforming is considered to be a key enabling technology for outdoor 5G mobile networks. Associated with beamforming, this paper investigates propagation power loss characteristics in two aspects. The first is beamwidth effects. Owing to the multipath receiving nature of mobile environments, it is expected that a narrower beamwidth antenna will capture fewer multipath signals, while increasing directivity gain. If we normalize the directivity gain, this narrow-beamwidth reception incurs an additional power loss compared to omnidirectional-antenna power reception. With measurement data collected in an urban area at 28 GHz and 38 GHz, we illustrate the amount of these additional propagation losses as a function of the half-power beamwidth. Secondly, we investigate power losses due to steering beam misalignment, as well as the measurement data. The results show that a small angle misalignment can cause a large power loss. Considering that most standard documents provide omnidirectional antenna path loss characteristics, these results are expected to contribute to mmWave mobile system designs.

Keywords: Beamforming, Channel measurements, Channel model, Millimeter wave, Multipath characteristics, Path loss.

I. Introduction

Owing to the vast spectrum availability in millimeter-wave (mmWave) bands, increasing attention has been given to mmWave 5G [1]–[9] (and references therein). In reviewing 5G requirements and visions [1]–[3], the authors study the necessity of mmWave introduction for 5G. With field measurements, the authors of [4]–[6] investigated mmWave propagation/channel characteristics and claimed that mmWave cellular networks can operate in outdoor small cells. mmWave system models and protocol designs for mobile networks were proposed in [7], [8]. In [9], industrial pre-5G developments were introduced.

A key enabling technology for reliable mmWave links is directional beamforming, which enables the overcoming of severe path loss at mmWave frequencies [4]. In this paper, we study additional power loss behaviors associated with this type of beamforming with respect to directional antenna reception: (1) beamwidth of directional beamforming (antennas) and (2) angle orientation (that is, beam-angle direction misalignment). Typical standard reports, such as those of the 3rd Generation Partnership Project (3GPP) [10], generally provide path loss parameters for only omnidirectional antennas. Thus, these beamwidth-dependent propagation behaviors will be useful tools in the design of mmWave systems. Considering the protocol overhead design for beam aligning, misalignment power loss characteristics will be useful as well. Based on field measurement data, we analyze these two effects of beamforming on propagation loss.

Manuscript received Sept. 15, 2017; revised Nov. 23, 2017; accepted Nov. 30, 2017.

This paper was presented in part at the IEEE 86th Vehicular Technology Conference, Toronto, Canada, Sept. 24–27, 2017 [24].

Juyul Lee (corresponding author, juyul@etri.re.kr), Myung-Don Kim (mdkim@etri.re.kr), and Jae-Joon Park (jjpark@etri.re.kr) are with the 5G Giga Service Research Laboratory, and Young Jun Chong (yjchong@etri.re.kr) is with the Broadcasting Media Research Laboratory, ETRI, Daejeon, Rep. of Korea.

To this end, we consider situations for directional antenna reception in multipath environments. (In typical cellular environments, mobile terminals receive numerous multipath signals from various directions). As shown in Fig. 1, the wedges depict the receiving antenna directivity; the arrows denote the incoming multipath signals. It is evident that the multipath receiving environments in Figs. 1(a) and (b) are the same; however, the beamwidths of the directional antennas are not. Here, $W_1 < W_2$ is shown; hence, it is expected that fewer multipath components will be received with the W_1 beamwidth antenna than with the W_2 beamwidth antenna. Consequently, a beamwidth-dependent power loss will occur, which will also be affected by the multipath environment.

In this paper, we first investigate this beamwidth-dependent power loss using 28 GHz and 38 GHz field measurement data collected in urban high-rise environments, where the beamwidth is parameterized by the half-power (3-dB) beamwidth (HPBW).

Another important issue when employing directional antennas and/or directional beamforming is beam misalignment. When the direction of the receiving antenna is not properly aligned, as illustrated in Fig. 2, power losses will occur. Based on the urban 28 GHz and 38 GHz measurement data, we investigate the amount of power losses as a function of this misalignment. Combined with the aforementioned beamwidth-dependent issue, the beam misalignment power loss is considered in terms of the directional antenna beamwidth. From our multipath-rich urban measurement data, we observe that the maximum power receiving direction is dependent on the beamwidth.

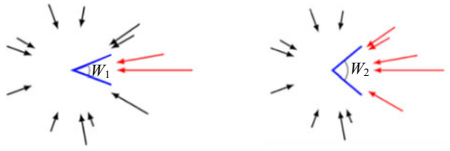

Fig. 1. Beamwidth effect on the number of multipath components affecting the received power loss ($W_1 < W_2$) with a (a) narrow-beamwidth antenna and (b) wide-beamwidth antenna.

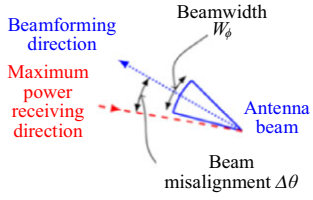

Fig. 2. Power loss in directional beamforming (antenna): beamwidth and misalignment.

Numerous measurements and channel modeling for frequencies above 6 GHz have been recently reported and proposed for standards [4]–[6] (and references therein). To develop harmonized common models, researchers in industry and academia have collectively published white papers [11]–[13]. Moreover, 3GPP announced its first release of channel models for frequencies above 6 GHz in [10], and ITU-R was in the process of developing a common model during the writing of this paper [12]. These channel models are important for system evaluations and sharing study (for new frequency allocations). However, to the best of our knowledge, all the standardized models provide only omnidirectional path loss characteristics as functions of distance and frequency. As a practical matter, directional beamforming is almost mandated for reliable mmWave links. Therefore, the omnidirectional characteristics may be inadequate for the design and evaluation of systems employing directional antennas (or beamforming). In this paper, we investigate the relation between the omnidirectional path loss and the directional path loss, wherein the directional path loss is loosely defined by path loss[1)] measured with directional antennas (or beamforming).

Regarding mmWave directional beamforming, surveys and a description of the underlying problems of beam misalignment were provided in [3]. Based on measurements in [14]–[17], the directional path loss was modeled in terms of the number of multipath components by considering the both coherent and non-coherent received power combining [18]. Theoretical analyses of beam misalignment with idealized antenna patterns were conducted in [19]–[22]. For a backhaul link, beam self-alignment with combined transmit–receive searching for proper beamforming patterns for multilevel codebook sets was investigated in [19]. Using a theoretical antenna pattern and a simulated multipath environment generated in [23], a lower and upper bound on the misalignment probability was investigated in [21] with consideration of the training sequence length and other system parameters. In 60-GHz line-of-sight (LOS) environments, the impacts of beam misalignment combined with the beamwidth were theoretically analyzed in [22]. Our measurement analysis, however, suggests that the received power is also affected by multipath environments.

Our analysis is based on 28 GHz and 38 GHz measurements collected in urban environments with two types of antennas: omnidirectional antennas and rotating

[1)] To describe directional path loss, path loss is used for the propagation loss between the transmitting power and the receiving power with antenna gain/calibration corrections; however, directionally isotropic transmission/reception is not assumed.

narrow-beamwidth horn antennas. We first show that the two antenna measurements are almost identical in an open space environment (no reflection/scattering/diffraction except for ground reflections) when the antenna pattern factors are properly considered. When similar measurements are held in urban areas (with rich reflection/scattering/diffraction environments), we show that the path loss measurements differ, even in LOS situations. By developing a beamwidth synthesis algorithm, we calculate the power loss in terms of beamwidth and misalignment angle.

Compared to our prior conference publication [24], this paper additionally includes power loss models developed with additional measurement data, including from a misalignment analysis. This misalignment issue is analyzed together with consideration of the beamwidth issue. (A simple aspect of the misalignment issue was analyzed in [25], [26] without consideration of the beamwidth.) It should be noted that our analyses are solely obtained from measurement data. Thus, the application may be limited when the environmental situations differ from our measurement setup. Hence, it is believed that the present analysis results can contribute to mmWave system development, such as feedback design, beamwidth determination, and coverage/interference analysis. Both 28 GHz and 38 GHz frequency bands are important 5G candidate bands. In 2016, Verizon [27] and Korea Telecom (KT) [28] released their own 5G specifications that can operate at 28 GHz. Moreover, ITU-R [29] and Federal Communications Commission (FCC) [30] announced 5G candidate frequencies between 24 GHz and 86 GHz, including 28 GHz[2] and 38 GHz bands.

II. Measurement Overview

1. Channel Sounder

We built a wideband channel sounder operating at 28 GHz and 38 GHz that can explore 500-MHz spatio-temporal characteristics. The multipath delay resolution is 2 ns and the path loss measurement range is 170 dB.[3] The sounder itself can transmit (equivalent isotropic radiated power (EIRP)) 29 dBm and 21 dBm for 28 GHz and 38 GHz measurements, respectively, and it can be amplified with directional antennas. As shown in Fig. 3,

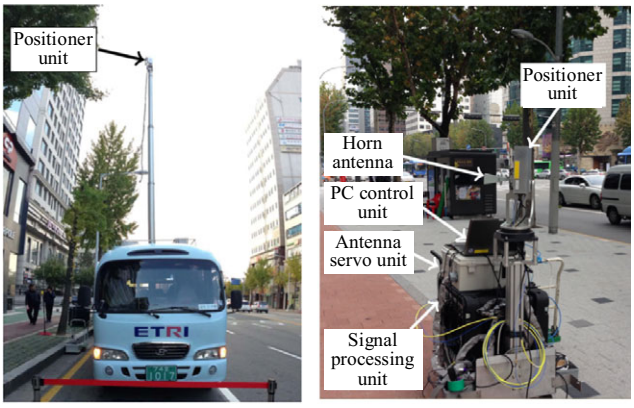

Fig. 3. 28 GHz and 38 GHz mmWave channel sounder system: (a) TX part and (b) RX part.

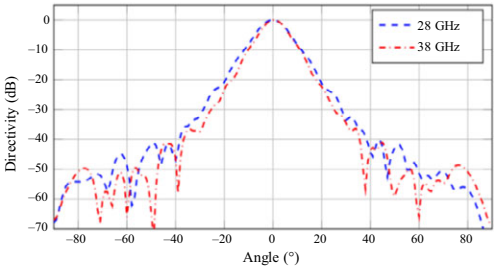

Fig. 4. Anechoic chamber antenna radiation pattern measurements of 10° HPBW antennas used for 28 GHz and 38 GHz measurements.

the sounder includes the following units for both TX and RX:

- Positioner unit, which includes 28 GHz and 38 GHz radio frequency (RF) modules and can support either a horn or an omnidirectional antenna.
- Antenna servo unit, which generates servo signals for horn antenna rotations with 1° accuracy.
- Signal processing unit, which performs intermediate frequency (IF)/baseband processing, including timing synchronization.
- PC control unit, which serves as the interface for operation/monitoring.

Figure 4 illustrates the anechoic chamber antenna pattern measurements of our 10° HPBW horn antennas. Their directivity gains are 24.40 dBi and 24.64 dBi for the 28 GHz and 38 GHz antennas, respectively.

2. Measurement Campaigns

We conducted measurement campaigns at two sites in the Republic of Korea: Buan and Daejeon. The Buan site is an open empty area; therefore, all links were LOS and

[2] To be specific, the ITU-R candidate band near 28 GHz is 24.25 GHz–27.5 GHz [29].

[3] This measurement range is calculated from the detectable channel impulse response (CIR) power range considering the automatic gain controller (AGC) dynamic range. For analysis, we used path loss data having less than 140 dB to provide a sufficient margin for the noise floor and other aspects.

https://doi.org/10.4218/etrij.2017-0188

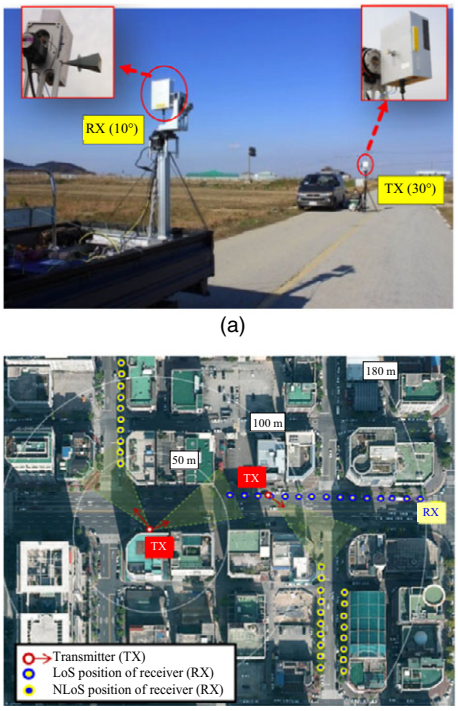

Fig. 5. Measurement site environments and scenarios: (a) Buan measurements and (b) Daejeon measurements.

were not disturbed by shielding materials (such as reflection/scattering objects) in the Fresnel zone. This resulted in two-ray propagation behavior. The Daejeon site is a typical urban area with rectangular street grids. Figure 5 shows the measurement site environments. Details are provided below.

A. Buan Measurements

Located in Jeonbuk Province, Republic of Korea, Buan comprises flat land that was reclaimed from the ocean for agricultural purposes. We placed the transmitter (TX) and receiver (RX) in an open area so that no objects, such as poles, buildings, trees, or traffic signs, could transgress the TX and RX measurement routes, as illustrated in Fig. 5(a). We fixed TX and moved RX along a straight-line path. We used a 30° HPBW antenna at the TX, as well as both a 10° HPBW horn and an omnidirectional antenna at the RX, in which all antennas were installed at a 2.5-m height.

B. Daejeon Measurements

The Daejeon measurements were obtained in the Dunsan district area, as shown in Fig. 5(b). It is a downtown area composed of flat, regular street grids (24 m–35 m street widths) surrounded by high-rise buildings (20 m–35 m building heights). The locations of TX and RX are marked in the figure depending on the LOS/NLOS scenarios. To emulate typical urban micro-cellular (UMi) scenarios, we installed the TX antenna at a 10-m height and the RX antenna at a 1.5-m height. At TX, we installed a 30° HPBW horn antenna. At RX, we installed both a 10° HPBW antenna and an omnidirectional antenna. The horn antenna was rotated at 10° steps. The number of measurement points and the measurement distance ranges are listed in Table 1.

Table 1. Number of TX-RX measurement samples and distance.

Freq. (GHz)	Link type	Ant. type	Buan measurements		Daejeon measurements	
			# pts	Distance (m)	# pts	Distance (m)
28	LOS	Omni	655	10–1,450	650	55–171
		Horn	2,970	12–1,940	24	55–171
	NLOS	Omni	N/A	N/A	700	43–127
		Horn	N/A	N/A	30	53–127
38	LOS	Omni	N/A	N/A	650	55–171
		Horn	1,882	10–1,745	24	55–171
	NLOS	Omni	N/A	N/A	700	43–127
		Horn	N/A	N/A	30	53–127

C. Measurement Considerations and Assumptions

Owing to time and equipment constraints, our measurements were conducted under several assumptions.

a. No elevation plane consideration

With our equipment, it required approximately 10 to 15 minutes in rotating a horn antenna through 360° in the azimuthal direction for a fixed elevation angle (36 steps with the 10° beamwidth antenna measurements). Considering the number of measurement points listed in Table 1, we rotated the horn antenna only in the azimuth direction while fixing the elevation angle to 0°. That is, our multipath component (MPC) analyses were performed in a two-dimensional manner, although the TX-RX separation distance was measured in a three-dimensional manner. The HPBWs (of our horn antennas) in the elevation direction were identical to those in the azimuth direction, that is, 10° HPBW.

b. Omnidirectional power radiation from TX

Although we were interested in the omnidirectional propagation characteristics, we installed a horn antenna at

the TX (while installing an omnidirectional antenna at the RX) to extend the range of the measurement distance. To mimic the omnidirectional antenna setup, however, we carefully chose the antenna location, beamwidth, and its boresight direction, including tilting angles associated with surrounding environments. Figure 5(b) shows the TX antenna beam direction in yellow shaded regions. We assumed that the same amount of radiation power would be directed if we installed an omnidirectional antenna at the same TX locations.

D. Stable Clock Synchronization between TX and RX

Although we were interested in the received power analysis in this study, we strived to achieve stable synchronization for power delay profile calculations. Both TX and RX parts of our sounder had rubidium clocks and auxiliary circuits for an absolute time reference and a pseudo-noise (PN) sequence synchronization between the TX and RX. We examined the time-dependent impacts on the synchronization accuracy when the TX and the RX rubidium clocks were disconnected. As depicted in Fig. 6, an approximately 9.5 ns (49.6 ns per 5 h) timing drift occurs every hour. This equates to approximately a 0.16 ns timing error occurring each minute. We believed that this would be acceptable for our power delay profile calculations.

E. Quasi-Static Environmental Variation during Horn-Antenna Rotation

We conducted major measurement campaigns in urban areas; nevertheless, we assumed that the multipath channel environments were static during a complete rotation of the horn antennas. By using a directional scanning method involving the rotating of a horn antenna, we are unable to capture MPCs simultaneously from all directions. To minimize the effects of environmental variations, we conducted the campaigns in a non-rush hour period when few pedestrians were on the sidewalk and the traffic was minimal.

Combined with a limited number of measurement sites, these assumptions may have limited the applicability of the analysis results. However, these same assumptions were widely accepted when measurement data were provided from rotating horn antenna measurements [4], [6], [14]–[19], [31]–[34].

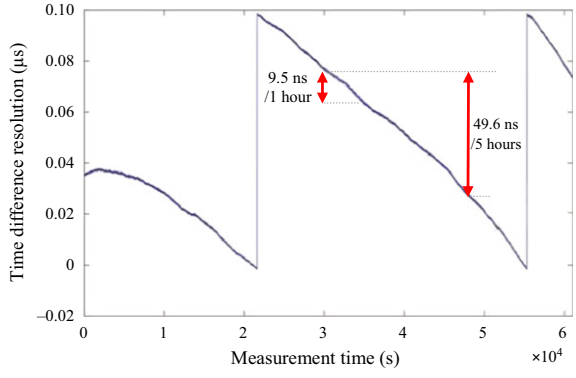

Fig. 6. Timing synchronization accuracy measurements.

III. Effects of Directional-Antenna Beamwidth on Received Power

This section investigates the beamwidth-dependent received power with our omnidirectional and horn-antenna measurements. Two examples are provided: (1) the case when the propagation loss of the omnidirectional measurements and those of the narrow-beamwidth horn antenna measurements were nearly identical to the Buan measurements (open areas); (2) the case when the two propagations differed from the Daejeon measurements (urban high-rise environments). By utilizing the measurement data, we developed an algorithm that synthesized an arbitrary beamwidth propagation loss and determined that the additional loss in the Daejeon measurements was due to the horn-antenna beamwidth. The synthesis algorithm is a modification of the omnidirectional synthesis algorithms in [32]–[35] with an incorporated beamwidth effect.

1. Directional-Antenna Measurements versus Omnidirectional-Antenna Measurements

We compared the directional-antenna measurements and the omnidirectional measurements collected in the two different environments: the open area (Buan measurement data) and the urban area (Daejeon data). It was expected that the measurements in the open area would follow the two-ray reflection model and would not be affected by the antenna beamwidth since there would be only two propagation paths incoming from the same direction. However, the urban measurements were expected to exhibit different behaviors since there would be numerous multipaths from various directions.

Figure 7 shows the 28 GHz open-area measurement data comparison along with the theoretical two-ray model over distances ranging from 1.4 km to 1.6 km. Since the TX and RX antenna heights are identical, denoted by h_{ant} in our measurement setup described in Section II-2, the two-ray model can be expressed as:

https://doi.org/10.4218/etrij.2017-0188

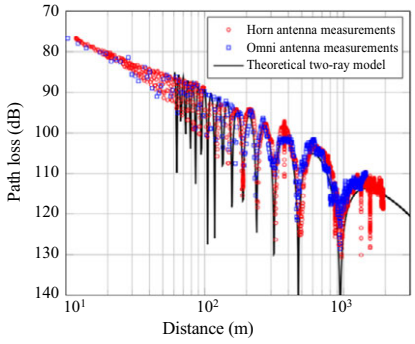

Fig. 7. Comparison between directional-antenna path loss and omnidirectional-antenna path loss with 28 GHz Buan measurements (open area).

$$\frac{1}{PL_{\text{two-ray}}(d)} = \left(\frac{\lambda}{4\pi}\right)^2 \left| \frac{e^{-j2\pi d}}{d} + \Gamma \frac{e^{-j2\pi\sqrt{d^2+\frac{4h_{\text{ant}}^2}{\lambda}}}}{\sqrt{d^2+4h_{\text{ant}}^2}} \right|^2, \quad (1)$$

where d is the TX-RX separation distance, λ is the wavelength, and Γ denotes the reflection coefficient. The two measurements show no meaningful difference; nonetheless, they nearly align with the theoretical model curve. It should be noted that open-area measurements with a single horn antenna at 60 GHz were shown in [36] and compared with those of the two-ray model. In this study, we employed not a single antenna, but two different beamwidth antennas, and we experimentally showed that the two measurements were identical in an open area.

Figure 8 shows the 28 GHz and 38 GHz Daejeon (urban) measurement data. The area is a typical multipath-rich environment, as described in Section II-2. The figure shows that the omnidirectional antenna measurements have smaller propagation losses than the horn antenna measurements on account of the spatial filtering of multipaths caused by the narrow-beamwidth antenna. To illustrate the multipath effects from our measurement data, we plotted the power angular delay profiles (PADP) shown in Fig. 9, which were captured at distances of 120 m for LOS and 80 m for NLOS in our 28 GHz data. These profiles show that multipath signals from various angle directions with different delays are incoming for both LOS and NLOS situations. Even in LOS, as shown in Fig. 9(a), we can observe that relatively strong signals are spread over some range of angles, which causes the difference between the horn antenna measurements and the omnidirectional antenna measurements. Since more multipath components are spread in NLOS, the difference

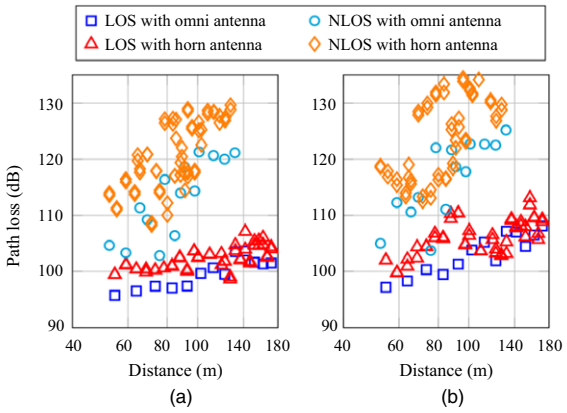

Fig. 8. Comparison between directional-antenna path loss and omni-directional-antenna path loss with the Daejeon (urban) measurements: (a) 28 GHz measurements and (b) 38 GHz measurements.

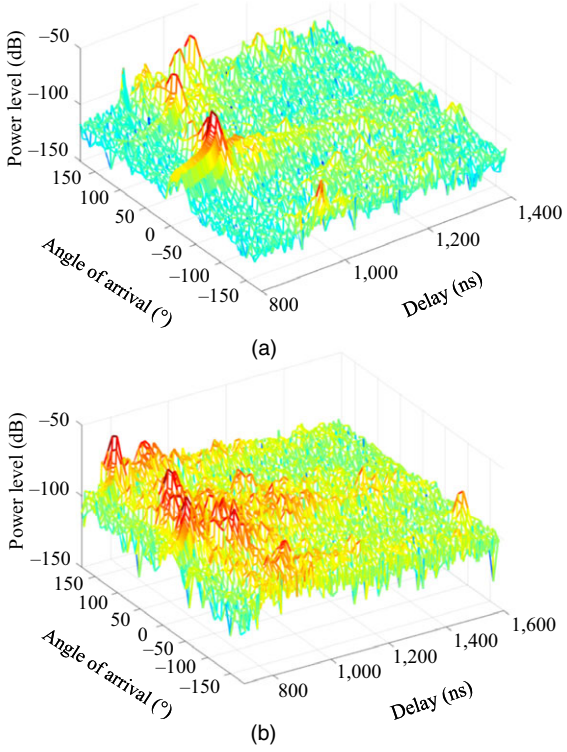

Fig. 9. Illustration of the power angular delay profile (PADP): (a) LOS and (b) NLOS.

between the omni-path loss and the horn-path loss will be larger, which agrees the results in Fig. 8.

Table 2 lists the quantitative differences between the two antenna measurements. The differences will be further evident by demonstrating that the differences between the synthesized omnidirectional characteristic from the horn antenna data and that of the actual omnidirectional data

Table 2. RMSD of the synthesized path loss from the actual measurements.

Freq. (GHz)	Link type	RMSD	
		Omni vs horn (dB)	Omni vs synthesized omni (dB)
28	LOS	2.76	0.91
	NLOS	7.38	3.00
38	LOS	3.25	1.82
	NLOS	6.84	2.98

become insignificant. As described in Section I, the directivity gain of the horn antenna was compensated when calculating the path loss. The boresight of the horn antenna was directed to the maximum power receiving direction for the horn-antenna measurements used in Fig. 8.

These two measurement results suggest that the propagation characteristics with a narrow-beamwidth directional antenna may not follow the omnidirectional characteristics, depending on the surrounding environment, even though most standards provide propagation characteristics only for omnidirectional antennas. In mmWave systems, to overcome severe free-space path losses, the use of high-gain (with a narrow beamwidth) directional beamforming (directional antennas) is generally unavoidable. From the perspective of system design and evaluation in mmWave systems, beamwidth-dependent propagation characteristics are to be considered in designing reliable mmWave links. To establish the relation between the omnidirectional propagation loss and the narrow-beamwidth characteristic, we developed a synthesis algorithm by utilizing the narrow-beamwidth horn antenna measurements given in the next subsection.

2. Beamwidth-Dependent Received Power Synthesization from Directional Antenna Measurements

In the development of standardized omnidirectional-antenna channel models, there have been several algorithm proposals for synthesizing omnidirectional characteristics from rotational scanning horn-antenna measurement data [32]–[35]. Although some differences exist, such as the level of information that is merged to yield synthesized characteristics, all proposed algorithms are limited because they are applicable only for omnidirectional characteristics, not for certain beamwidth characteristics. Based on the general ideas in [32]–[35], however, we devised an arbitrary beamwidth synthesizing algorithm by including an estimation of the boresight direction to maximize the received power with a given beamwidth. To estimate the maximum received power direction for a given beamwidth, our algorithm was developed to synthesize the power sum from the PADP over the beamwidth interval.

In our measurement setup specified in Section II-2, both the beamwidth of the horn antenna and its rotation step were set to 10° for non-overlapping scanning. We devised the positioner to align the rotational axes (both horizontal and vertical directions) to the horn antenna vertex. With this positioner rotation and a proper synthesis algorithm, which are discussed below, Fig. 10 shows the synthesized antenna pattern compared with the original horn antenna pattern. The horn antenna pattern is from our 28 GHz 10° HPBW antenna shown in Fig. 4. The synthesized antenna pattern has ripples, as shown in Fig. 10, since we rotated it in 10° steps. If we rotated it with a smaller step, the synthesized pattern would be close to a circle. Considering the measurement and data processing limitations, we assumed that the effects of these ripples were negligible.

We now consider an algorithm for beamwidth-dependent propagation loss. Let $h_\phi(\tau)$ be the channel impulse response (CIR) of the azimuthal angle ϕ direction. Then, the ϕ-directional power delay profile can be obtained by squaring the CIR:

$$\mathrm{PDP}_\phi(\tau) = |h_\phi(\tau)|^2. \tag{2}$$

The $\mathrm{PDP}_\phi(\tau)$ can be viewed as a power angular delay profile (PADP) when ϕ is measured in sufficiently small steps. The relationship to the regular PDP can be obtained by

$$\mathrm{PDP}(\tau) = \int_\varphi \mathrm{PDP}_\varphi(\tau) \sum_{k=1}^{K} \Omega(\varphi - k\omega), \tag{3}$$

where K and ω denote the number of rotation steps and the rotation step size, respectively, and $\Omega(\cdot)$ denotes the horn antenna pattern. Figure 11 illustrates a comparison of the actual omnidirectional PDP measurements and the synthesized PDP measurements using the PADP data shown in Fig. 9. It is apparent that, in both LOS and NLOS cases, the dominant components are well matched.

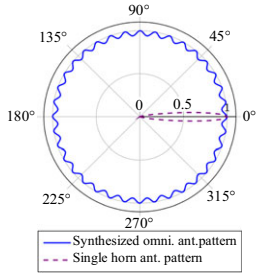

Fig. 10. Synthesized (normalized) antenna patterns.

To minimize the effects of noise and spurious signals, we set the threshold from the peak power and also from the noise floor level, as suggested in Recommendation ITU-R P.1407 [37], where the thresholded PDP is denoted by $\widetilde{\mathrm{PDP}}_\phi(\tau)$. By integrating $\widetilde{\mathrm{PDP}}_\phi(\tau)$ delay τ, we can calculate the received power for direction ϕ as:

$$P_\phi = \int_\tau \widetilde{\mathrm{PDP}}_\phi(\tau). \tag{4}$$

Next, we strive to identify the maximum received power direction for a given beamwidth, W_ϕ, which can be obtained by maximizing the integrated power in angle domain within a W_ϕ range:

$$\hat{\phi}_{\mathrm{peak}} = \arg\max_\phi \int_{\varphi=\phi-\frac{W_\phi}{2}}^{\phi+\frac{W_\phi}{2}} P_\varphi \sum_{k=1}^{K} \Omega(\varphi - k\omega). \tag{5}$$

Note that $\hat{\phi}_{\mathrm{peak}}$, the maximum received power direction, depends on beamwidth W_ϕ. Then, we calculate the synthesized the W_ϕ beamwidth received power as:

$$P_{W_\phi} = \int_{\varphi=\hat{\phi}_{\mathrm{peak}}-\frac{W_\phi}{2}}^{\hat{\phi}_{\mathrm{peak}}+\frac{W_\phi}{2}} P_\varphi \sum_{k=1}^{K} \Omega(\varphi - k\omega). \tag{6}$$

The conventional path loss can be calculated as:

$$L(d, W_\phi) = 10\log_{10}\frac{P_{W_\phi}}{P_{\mathrm{transmit}}} + \xi, \tag{7}$$

where P_{transmit} and ξ denote the transmit power and the correction/impairments (such as the cable loss, antenna gain), respectively. Using the synthesis algorithm, the original horn-versus-omni comparison shown in Fig. 8 changes to Fig. 12, where the two measurements are comparable. The root-mean-square-difference (RMSD) is listed in Table 2.

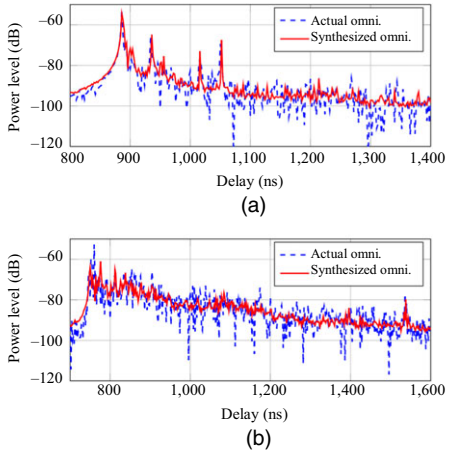

Fig. 11. PDP comparison with the data shown in Fig. 9: (a) LOS and (b) NLOS.

Note that we provide the assessment of the synthesis algorithm by comparing with our actual omnidirectional antenna measurements. Although [32]–[35] proposes omnidirectional synthesis algorithms, they do not provide comparisons with actual omnidirectional measurements.

3. Propagation Loss as a Function of Beamwidth

We write the overall propagation loss, in dB domain, as a sum of omnidirectional-antenna path loss L^{omni} and narrow-beamwidth beamforming loss ΔL^{BW}:

$$L^{\mathrm{overall}}(d, W_\phi) = L^{\mathrm{omni}}(d) + \Delta L^{\mathrm{BW}}(W_\phi)(\mathrm{dB}). \tag{8}$$

Since L^{omni} can be referred to the typical omnidirectional path loss models such as [10], [38], our focus is on the additional loss term ΔL^{BW}. By examining our measurement data, we observed that this additional loss does not depend on the TX-RX distance (Figure 13 shows that ΔL^{BW}'s at d = 65 m, 100 m, 130 m are overlapped for all scenarios). In fact, the distance factor is captured in L^{omni}. We also observe that the additional loss term is inversely related to the beamwidth. Thus, we consider the following model and fit it with our measurements:

$$\Delta L^{\mathrm{BW}}(W_\phi) = \eta\left(\frac{1}{W_\phi} - \frac{1}{360^\circ}\right), 10^\circ \le W_\phi \le 360^\circ, \tag{9}$$

where W_ϕ denotes HPBW in degrees. The fitting results are listed in Table 3 and plotted in Fig. 13. These fitting results are limited to applications in urban environments since this additional loss is a multipath-related factor affected by the receiver surrounding environment. As observed in the fitting plots, the model agrees with the field measurement data.

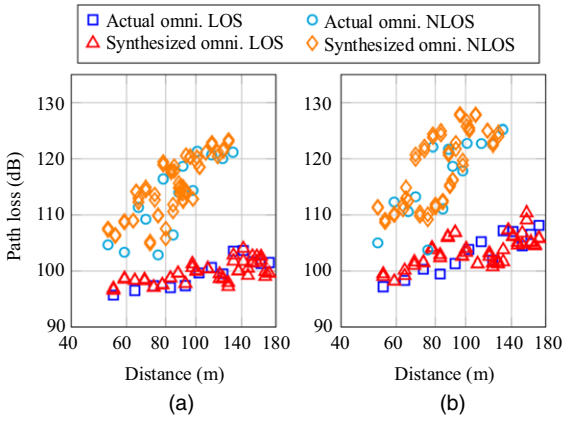

Fig. 12. Omni-directional path loss: Omni-directional antenna measurements versus synthesis results from horn antenna measurements: (a) 28 GHz measurements and (b) 38 GHz measurements.

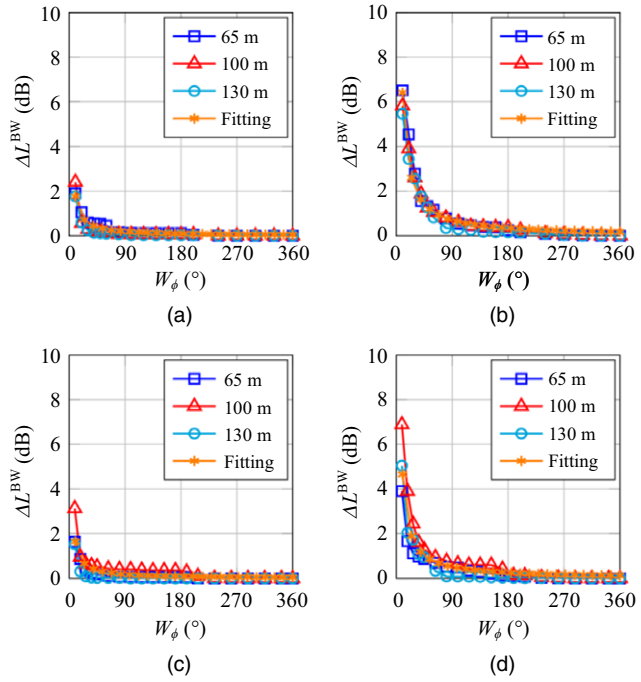

Fig. 13. Beamwidth dependency of the additional path loss: (a) 28 GHz LOS, (b) 28 GHz NLOS, (c) 38 GHz LOS, and (d) 38 GHz NLOS.

IV. Power Loss due to Beam Misalignment

This section investigates another aspect of additional propagation loss due to beam misalignment, which is also associated with beamforming (directional antenna uses). This additional loss, denoted by $\Delta L^{\text{mis-aligned}}$, is defined by the deviation from the maximum received power:[4)]

$$\Delta L^{\text{mis-aligned}}(\theta, d, W_\phi) = L(\theta, d, W_\phi) \underbrace{- \min_{\theta} L(\theta, d, W_\phi)}_{\text{peak power at } d \text{ with beamwidth } W_\phi}, \quad (10)$$

where $L(\theta, d, W_\phi)$ denotes the W_ϕ beamwidth directional propagation loss at rotational angle θ and distance d. The second term, minimizing L with respect to θ, corresponds to the maximum power at distance d and with beamwidth W_ϕ. It would be more appropriate to express $\Delta L^{\text{misaligned}}$ in terms of misaligned angle $\Delta\theta$, which can be calculated by

$$\Delta\theta(\theta, d, W_\phi) = \theta - \arg\min_{\theta} L(\theta, d, W_\phi). \quad (11)$$

The beam misalignment issue combined with the beamwidth is now examined. In Section III-2, it was shown that the maximum received power direction is dependent on beamwidth W_ϕ, even in LOS environments, as shown in Fig. 14.

Table 3. Fitting parameter η for urban environments.

Freq. (GHz)	Link type	η	RMSE (dB)
28	LOS	17.70	0.16
	NLOS	64.03	0.33
38	LOS	16.44	0.25
	NLOS	46.49	0.42

Figure 15 shows the measurements of additional power loss due to beam misalignment. We can observe that the average power loss is almost symmetric with respect to $\Delta\theta$. The power loss increases as $|\Delta\theta|$ increases and becomes saturated for a large $|\Delta\theta|$, whose value depends on beamwidth W_ϕ. When the beamwidth is small, a slight misalignment incurs considerable power loss. We can also observe that the power loss is inversely proportional to the beamwidth. Based on these observations, we consider the following model:

$$\Delta L^{\text{misaligned}} = \begin{cases} \mu|\Delta\theta|\left(\frac{1}{W_\phi} - \frac{1}{360^\circ}\right), & \frac{|\Delta\theta|}{W_\phi} \le \zeta, W_\phi \le W_{\text{lim}} \\ \nu\left(\frac{1}{W_\phi} - \frac{1}{360^\circ}\right), & \frac{|\Delta\theta|}{W_\phi} > \zeta, W_\phi \le W_{\text{lim}} \\ 0, & W_\phi > W_{\text{lim}}, \end{cases} \quad (12)$$

where μ, ν, ζ, and W_{lim} are model fitting parameters. Their fitting results are listed in Table 4.

Figure 16 illustrates how the misaligned power loss behaves in terms of the misaligned angle $\Delta\theta$ when the beamwidth is fixed to $W_\phi = 10^\circ$ (we select $W_\phi = 10^\circ$ for illustration since the HPBW of the antenna is also 10°) along with the antenna pattern. Owing to the multipath nature of the measurement environments, the increment of the additional loss with respect to $\Delta\theta$ is smaller than the antenna pattern behavior. This behavior is more evident in NLOS situations. This implies that the beam misalignment analysis performed solely with antenna patterns may produce erroneous results, especially when numerous multipaths are received from various directions. The

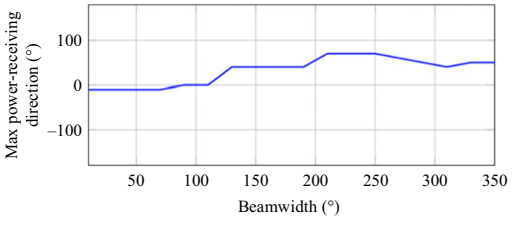

Fig. 14. Beamwidth-dependent maximum power-receiving direction for the LOS in Fig. 9(a).

[4)] The maximum power reception occurs when the propagation loss is minimized.

https://doi.org/10.4218/etrij.2017-0188

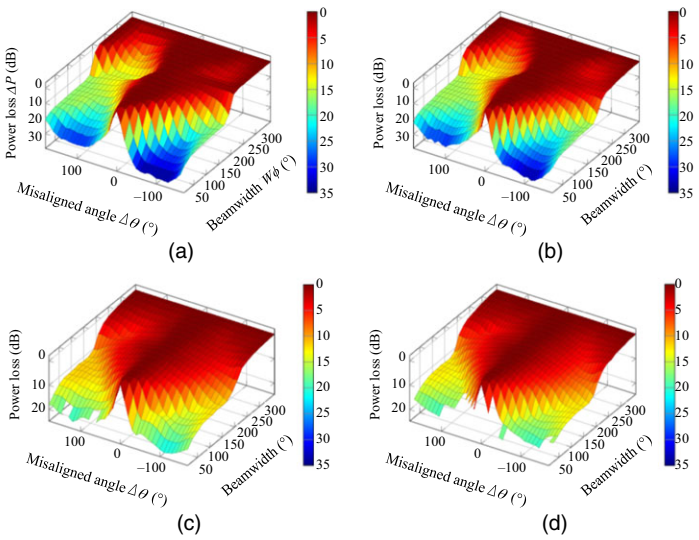

Fig. 15. Average power loss with respect to both misaligned angle and beamwidth from our measurement data: (a) 28 GHz LOS (b) 38 GHz LOS, (c) 28 GHz NLOS, and (d) 38 GHz NLOS.

Table 4. Beam misalignment power loss fitting parameters for urban environments.

Freq. (GHz)	Link type	Fitting parameters				RMSE (dB)
		μ (dB)	v (dB/°)	ζ	W_{lim} (°)	
28	LOS	3.75	62.12	68.79	239.69	9.21
	NLOS	2.37	62.11	68.77	239.69	5.29
38	LOS	3.34	62.11	68.78	239.68	8.83
	NLOS	3.23	62.11	68.78	239.68	5.25

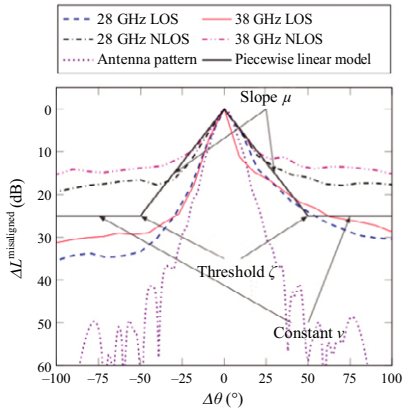

Fig. 16. Beam misaligned power loss behavior (for a fixed beamwidth) with respect to misaligned angle in an urban environment.

model in (12) can be depicted in a piecewise linear model for a fixed beamwidth, as Fig. 16 shows.

Figure 17 shows the behavior of the misaligned power loss in terms of beamwidth W_ϕ for fixed misaligned angles

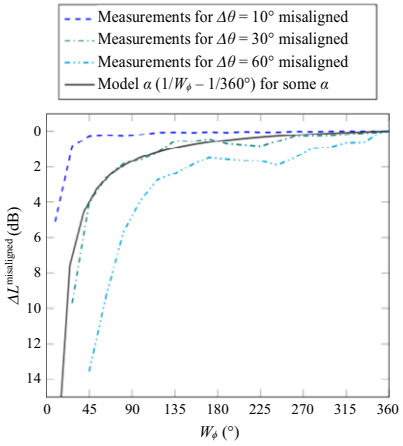

Fig. 17. Beam misaligned power loss behavior (for fixed misaligned angles) with respect to beamwidth from the 38 GHz NLOS urban measurements.

$\Delta\theta = 10^\circ$, 30°, and 60°. We also plot the model in (12) for a fixed $\Delta\theta$ to illustrate the validity of the model compared with the measurement results. In both Figs. 16 and 17, it is evident that a considerable power loss can result with a small beam misalignment, especially when the beamwidth is small.

V. Conclusion

Based on mmWave measurement data analysis, we investigated two aspects of additional power losses that can occur with directional beamforming, specifically with directional antennas. The first was the beamwidth effect associated with multipath-rich propagation environments. We observed that a narrowing beamwidth can decrease the

power reception on account of the spatial filtering of multipath components. Usually, it is advised that high-gain directional beamforming (by narrowing the beamwidth) is employed in an mmWave system design to overcome severe free-space loss. However, our observation revealed the requirement to balance the directivity gain increases (with a narrowing beamwidth) against the power loss due to this narrowing beamwidth. The second aspect was the effect of beam misalignment. Our analysis results showed that more precise beam alignment is required for smaller beamwidth antennas. Considering that directional (narrow-beamwidth) beamforming is expected to be employed for 5G mmWave mobile systems, we believe that these investigations will be helpful for predicting more accurate propagation behaviors.

Acknowledgements

This work was supported by the Institute for Information and Communications Technology Promotion (IITP) grant funded by the Korean government (MSIT) (2017-0-00066, "Development of time-space based spectrum engineering technologies for preemptive use of frequency") and (B0101-16-222, "Development of core technologies to improve spectral efficiency for mobile big-bang").

References

[1] J.G. Andrews et al., "What Will 5G Be?" *IEEE J. Sel. Areas Commun.*, vol. 32, no. 6, June 2014, pp. 1065–1082.

[2] F. Boccardi, R.W. Heath, A. Lozano, T.L. Marzetta, and P. Popovski, "Five Disruptive Technology Directions for 5G," *IEEE Commun. Mag.*, vol. 52, no. 2, Feb. 2014, pp. 74–80.

[3] M. Agiwal, A. Roy, and N. Saxena, "Next Generation 5G Wireless Networks: A Comprehensive Survey," *IEEE Commun. Surveys Tutorials*, vol. 18, no. 3, 2016, pp. 1617–1655.

[4] T.S. Rappaport et al., "Millimeter Wave Mobile Communications for 5G Cellular: It Will Work!" *IEEE Access*, vol. 1, May 2013, pp. 335–349.

[5] T.S. Rappaport et al., *Millimeter Wave Wireless Communications*, Prentice Hall, 2014.

[6] J. Lee, J. Liang, M. Kim, J. Oark, B. Park, and H.K. Chung, "Measurement-Based Propagation Channel Characteristics for Millimeter-Wave 5G Giga Communication Systems," *ETRI J.*, vol. 38, no. 6, Dec. 2016, pp. 1031–1041.

[7] C. Dehos, J.L. González, A. De Domenico, D. Kténas, and L. Dussopt, "Millimeter-Wave Access and Backhauling: The Solution to the Exponential Data Traffic Increase in 5G Mobile Communications Systems?" *IEEE Commun. Mag.*, vol. 52, no. 9, Sept. 2014, pp. 88–95.

[8] J.G. Andrews, T. Bai, M.N. Kulkarni, A. Alkhateeb, A.K. Gupta, and R.W. Heath, "Modeling and Analyzing Millimeter Wave Cellular Systems," *IEEE Trans. Commun.*, vol. 65, no. 1, Jan. 2017, pp. 403–430.

[9] J. Gozalvez, "Prestandard 5G Developments," *IEEE Veh. Tech. Mag.*, vol. 9, no. 4, Dec. 2014, pp. 14–28.

[10] 3GPP TR 38.900, *Study on Channel Model for Frequency Spectrum above 6 GHz (Release 14)*, June 2016.

[11] Aalto University et al., *5G Channel Models for Bands up to 100 GHz*, White Paper Rev. 2.0, Mar. 2016. http://www.5gworkshops.com/5GCM.html

[12] ITU-R Doc 3K/73-E (2016), *Chairman's Report on the Meeting of Working Party 3K* (Geneva, Switzerland, 20–29 June 2016), Source: Chairman, Aug. 2016.

[13] 5G Millimeter-Wave Channel Model Alliance, *5G Alliance Working Group–GLOBECOM Meeting*, Meeting Slides, Dec. 2016.

[14] T.S. Rappaport, G.R. MacCartney, M.K. Samimi, and S. Sun, "Wideband Millimeter-Wave Propagation Measurements and Channel Models for Future Wireless Communication System Design," *IEEE Trans. Commun.*, vol. 63, no. 9, Sept. 2015, pp. 3029–3056.

[15] E. Ben-Dor, T.S. Rappaport, Y. Qiao, and S.J. Lauffenburger, "Millimeter-Wave 60 GHz Outdoor and Vehicle AOA Propagation Measurements Using a Broadband Channel Sounder," in *Proc. IEEE Globecom Conf.*, Houston, TX, USA, Dec. 2011, pp. 1–6.

[16] G.R. MacCartney Jr. and T.S. Rappaport, "73 GHz Millimeter Wave Propagation Measurements for Outdoor Urban Mobile and Backhaul Communications in New York City," in *Proc. IEEE Int. Conf. Commun.*, Sydney, Australia, June 2014, pp. 4862–4867.

[17] T.S. Rappaport, E. Ben-Dor, J.N. Murdock, and Y. Qiao, "38 GHz and 60 GHz Angle-Dependent Propagation for Cellular & Peer-to-Peer Wireless Communications," in *Proc. IEEE Int. Conf. Commun.*, Ottawa, Canada, June 2012, pp. 4568–4573.

[18] A.I. Sulyman, A. Alwarafy, G.R. MacCartney, T.S. Rappaport, and A. Alsanie, "Directional Radio Propagation Path Loss Models for Millimeter-Wave Wireless Networks in the 28-, 60-, and 73-GHz Bands," *IEEE Trans. Wireless Commun.*, vol. 15, no. 10, Oct. 2016, pp. 6939–6947.

[19] S. Hur, T. Kim, D.J. Love, J.V. Krogmeier, T.A. Thomas, and A. Ghosh, "Multilevel Millimeter Wave Beamforming for Wireless Backhaul," in *Proc. IEEE Globecom Workshops Femtocell Netw.*, Houston, TX, USA, Dec. 2011, pp. 253–257.

[20] H. Yang, M.H.A.J. Herben, I.J.A.G. Akkermans, and P.F.M. Smulders, "Impact Analysis of Directional Antennas and Multiantenna Beamformers on Radio Transmission," *IEEE Trans. Veh. Tech.*, vol. 57, no. 3, May 2008, pp. 1695–1707.

[21] C. Liu et al., "Millimeter Wave Beam Alignment: Large Deviations Analysis and Design Insights," Nov. 2016, Accessed 2017. http://arxiv.org/abs/1611.04212/

[22] G. Yang, J. Du, and M. Xiao, "Analysis on 60 GHz Wireless Communications with Beamwidth-Dependent Misalignment," Nov. 2016, Accessed 2017. http://arxiv.org/abs/1611.07867

[23] NYU Wireless, *NYUSIM: The Open Source 5G Channel Model Simulator Software*, July 2016, Accessed 2017. http://wireless.engineering.nyu.edu/5g-millimeter-wave-channel-modeling-software/

[24] J. Lee et al., "Beamwidth-Dependent Directional Propagation Loss Analysis Based on 28 and 38 GHz Urban Micro-Cellular (UMi) Measurements," in *Proc. IEEE VTC 2017 Fall*, Toronto, Canada, Sept. 2017.

[25] J. Lee et al., "Millimeter-Wave Beam Mis-Alignment Analysis Based on 28 and 38 GHz Urban Measurements," in *Proc. IEEE VTC 2017 Fall*, Toronto, Canada, Sept. 2017.

[26] J. Lee et al., "Power Losses due to Steering Beam Misalignment in Directional-Antenna Millimeter-Wave Systems," in *Proc. URSI Asia-Pacific Radio Science Conference*, Seoul, Rep. of Korea, Aug. 2016, pp. 609–610.

[27] Verizon 5G Technical Forum, Accessed 2017. http://www.5gtf.org

[28] KT 5G-SIG, Accessed 2017. http://www.kt.com/eng/biz/kt5g 02.jsp

[29] ITU, "Provisional Final Acts," The World Radio Communication Conference (WRC-15): Resolution COM 6/20, Nov. 2015.

[30] FCC Doc-339990A1. "Fact Sheet: Spectrum Frontiers Proposal to Identify, Open Up Vast Amounts of New High-band Spectrum for Next Generation (5G) Wireless Broadband, Accessed 2017. https://apps.fcc.gov/edocs_public/attachmatch/DOC-339990A1.pdf

[31] S. Sun et al., "Investigation of Prediction Accuracy, Sensitivity, and Parameter Stability of Large-Scale Propagation Path Loss Models for 5G Wireless Communications," *IEEE Trans. Veh. Tech.*, vol. 65, no. 5, May 2016, pp. 2843–2860.

[32] S. Sun, G.R. MacCartney, M.K. Samimi, and T.S. Rappaport, "Synthesizing Omnidirectional Antenna Patterns, Received Power and Path Loss from Directional Antennas for 5G Millimeter-Wave Communications," in *Proc. IEEE Globecom Conf.*, San Diego, CA, USA, Dec. 2015, pp. 1–7.

[33] K. Haneda, S.L.H. Nguyen, J. Järveläinen, and J. Putkonen, "Estimating the Omni-Directional Pathloss from Directional Channel Sounding," in *Proc. Eur. Conf. Antennas Propag.*, Davos, Switzerland, Apr. 2016, pp. 1–5.

[34] S. Salous, X. Raimundo, and A. Cheema, "Path Loss Model in Typical Outdoor Environments in the 50–73 GHz Band," in *Proc. Eur. Conf. Antennas Propag.*, Paris, France, Mar. 2017, pp. 721–724.

[35] ITU-R Doc 3J/34-E, (2016), "Proposed Revision to Recommendation ITU-R P.1407-5: Multipath Propagation and Parametrisation of its Characteristics–Directional Multipath Parameters," Source: UK and Northern Ireland, June 2016.

[36] R.J. Weiler, M. Peter, W. Keusgen, A. Kortke, and M. Wisotzki, "Millimeter-Wave Channel Sounding of Outdoor Ground Reflections," in *Proc. IEEE Radio and Wireless Symposium (RWS)*, San Diego, CA, USA, Jan. 2015, pp. 95–97.

[37] Rec. ITU-R P.1407-6, "Multipath Propagation and Parameterization of Its Characteristics," ITU, June 2017.

[38] Rec. ITU-R P.1411-9, "Propagation Data and Prediction Methods for the Planning of Short-Range Outdoor Radiocommunication Systems and Radio Local Area Networks in the Frequency Range 300 MHz to 100 GHz," ITU, June 2017.

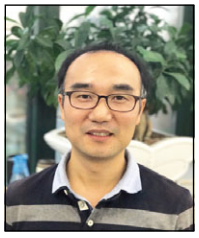

Juyul Lee received his PhD degree in electrical engineering from the University of Minnesota, Twin Cities, USA, in 2010. He was with the Agency for Defense Development, Daejeon, Rep. of Korea from 1998 to 2000. Since 2000, he has been with the ETRI, Daejeon, Rep. of Korea, where he is currently a principal researcher at the 5G Giga Service Research Laboratory. His research interests include millimeter-wave channel measurements and modeling. He has contributed to ITU-R recommendations and reports in Study Group 3 (Propagation), including millimeter-wave propagation models. He is currently the chairman of the ITU-R Correspondence Group 3K-6, which studies the impact of higher frequencies (from 6 GHz to 100 GHz) on propagation models and related characteristics.

Myung-Don Kim received his BS and MS degrees in electronics engineering from Dong-A University, Busan, Rep. of Korea, in 1993 and 1995, respectively. Since 1995, he has been with the ETRI, Daejeon, Rep. of Korea, where he is currently a principal researcher and a managing director of the Mobile RF Research Section. Since 2006, he has

participated in a project on the development of wideband channel sounder and channel models for microwave and millimeter-wave wireless communications. His research interests include radio propagation, field measurement, channel modeling, and radio frequency technologies for next-generation wireless communications.

Jae-Joon Park received his BS and MS degrees in control and instrumentation from Chung-Ang University, Seoul, Rep. of Korea in 1997 and 1999, respectively. He is a principal researcher of the ETRI, Daejeon, Rep. of Korea. Since 1999, he has participated in the project on the development of smart antennas for FDD/TDD WCDMA systems, the Wireless Broadband (WiBro) system, and wideband wireless channel models for next-generation mobile communications. His current research interests are channel modeling for millimeter-wave high-speed vehicular wireless communications.

Young Jun Chong received a BS degree in electronics engineering from Jeju University, Rep. of Korea, in 1992, an MS degree in electronics engineering in 1994 from Sogang University, Seoul, Rep. of Korea, and a PhD degree in electronic engineering from Chungnam National University, Daejeon, Rep. of Korea, in 2005. Since 1994, he has been with ETRI, Daejeon, Rep. of Korea, where he is currently a principal researcher. He served as a managing director of the spectrum engineering research team. His research interests include radio frequency circuits and systems, radio interference, mobile communications, and interference modeling.

https://doi.org/10.4218/etrij.2017-0188